Calorimetric Studies of Ligand Binding in R67 Dihydrofolate Reductase†

Michael Jackson,‡ Shaileja Chopra,‡ R. Derike Smiley,‡,§ Patrick O'Neal Maynord,‡ Andre Rosowsky,|| Robert E. London,⊥ Louis Levy,⊥ Thomas I. Kalman,# and Elizabeth E. Howell*,‡

Department of Biochemistry, Cellular, and Molecular Biology, University of Tennessee, Knoxville, Tennessee 37996-0840, Laboratory of Structural Biology, MR-01, National Institute of Environmental Health Sciences, National Institutes of Health, Box 12233, Research Triangle Park, North Carolina 27709, Dana-Farber Cancer Institute and Department of Biological Chemistry and Molecular Pharmacology, Harvard Medical School, Boston, Massachusetts 02115, and Department of Chemistry, University at Buffalo, 457C Cooke Hall, Amherst, New York 14260

Received May 12, 2005; Revised Manuscript Received July 19, 2005

ABSTRACT: R67 dihydrofolate reductase (DHFR) is a novel bacterial protein that possesses 222 symmetry and a single active site pore. Although the 222 symmetry implies that four symmetry-related binding sites must exist for each substrate as well as for each cofactor, various studies indicate only two molecules bind. Three possible combinations include two dihydrofolate molecules, two NADPH molecules, or one substrate plus one cofactor. The latter is the productive ternary complex. To explore the role of various ligand substituents during binding, numerous analogues, inhibitors, and fragments of NADPH and/or folate were used in both isothermal titration calorimetry (ITC) and K_i studies. Not surprisingly, as the length of the molecule is shortened, affinity is lost, indicating that ligand connectivity is important in binding. The observed enthalpy change in ITC measurements arises from all components involved in the binding process, including proton uptake. As a buffer dependence for binding of folate was observed, this likely correlates with perturbation of the bound N3 pK_a, such that a neutral pteridine ring is preferred for pairwise interaction with the protein. Of interest, there is no enthalpic signal for binding of folate fragments such as dihydrobiopterin where the *p*-aminobenzoylglutamate tail has been removed, pointing to the tail as providing most of the enthalpic signal. For binding of NADPH and its analogues, the nicotinamide carboxamide is quite important. Differences between binary (binding of two identical ligands) and ternary complex formation are observed, indicating interligand pairing preferences. For example, while aminopterin and methotrexate both form binary complexes, albeit weakly, neither readily forms ternary complexes with the cofactor. These observations suggest a role for the O4 atom of folate in a pairing preference with NADPH, which ultimately facilitates catalysis.

Dihydrofolate reductase (DHFR)[1] catalyzes the transfer of a hydride ion from nicotinamide adenine dinucleotide phosphate (NADPH) to dihydrofolate (DHF). The product, tetrahydrofolate (THF), is an essential cofactor in the biosynthesis of thymidylate, methionine, purine nucleotides, and other metabolites. Inhibition of this enzyme arrests DNA synthesis and cell division leading to cell death; thus chromosomal DHFRs have become targets for antifolate drugs in the treatment of cancer as well as bacterial and parasitic infections (*1*, *2*). Trimethoprim (TMP) is a clinically important inhibitor of bacterial DHFRs. R67 DHFR is a type II, R-plasmid-encoded enzyme, conferring resistance to TMP. Most plasmid-encoded DHFRs show sequence homology with chromosomal DHFRs; however, R67 DHFR possesses neither sequence nor structural similarity with the chromosomal enzyme (*3*, *4*). A recent review compares these two different DHFRs (*5*).

The crystal structures of apo R67 DHFR and of an R67 DHFR·folate complex have been determined (1VIE and 1VIF in the Protein Data Bank) (*4*). R67 DHFR is a homotetramer. Each monomer is 78 amino acids long and forms a five-stranded β-barrel as seen in SH3 domains. As

† This work was supported by NSF Grant MCB-0445728.

* Corresponding author: phone, 865-974-4507; fax, 865-974-6306; e-mail, lzh@utk.edu.

‡ University of Tennessee.

§ Present address: Department of Biochemistry, Duke University Medical Center, Box 3711, Durham, NC 27710.

|| Harvard Medical School.

⊥ National Institute of Environmental Health Sciences, NIH.

University at Buffalo.

[1] Abbreviations: R67 DHFR, R67 dihydrofolate reductase; wt, wild type; ITC, isothermal titration calorimetry; NADPH, nicotinamide adenine dinucleotide phosphate, reduced; NADH, nicotinamide adenine dinucleotide, reduced; NHDPH, nicotinamide hypoxanthine dinucleotide phosphate, reduced; ATP-ribose, 2′-monophosphoadenosine 5′-diphosphoribose; ADP-ribose, adenosine 5′-diphosphoribose; NMNH, nicotinamide mononucleotide phosphate, reduced; 2′,5′-ADP, 2′,5′-diphosphoadenosine; AcPADPH, acetylpyridine adenine dinucleotide phosphate, reduced; DHF, 7,8-dihydrofolate; THF, 5,6,7,8-tetrahydrofolate; pABA-Glu, *p*-aminobenzoylglutamate tail of folate; PG2, pteroyldi-γ-L-glutamate; PG5, pteroylpenta-γ-L-glutamate; DHB, dihydrobiopterin; DHP, dihydropteroic acid; TMP, trimethoprim; MTX, methotrexate; ADMDF, 2-aza-2-deamino-N^{10}-methyl-5,8-dideazafolic acid; N5DHC, N^{α}-(5-deazapteroyl)-L-homocysteic acid; N5DAPB, D,L-2-[*N*-(5-deazapteroyl)amino]-4-phosphobutanoic acid; THFAC, (6*R*,6*S*)-N^{α}-(5-deaza-5,6,7,8-tetrahydropteroyl)-L-homocysteic acid; TDTHF, (6*R*,6*S*)-5,8,10-trideaza-5,6,7,8-tetrahydropteroyl-L-glutamic acid; PT648, (2*S*)-2-[5-[*N*-(2-amino-4(3*H*)-oxopyrido[2,3-*d*]pyrimidin-6-yl)methylamino]-2,3-dihydro-1(3*H*)-oxoisoindol-2-yl]aminopentane-1,5-dioic acid; PT489, N^{α}-pteroyl-L-ornithine; DMDDF, 2-deamino-2-methyl-5,8-dideazafolate; MTA buffer, 100 mM Tris, 50 mM Mes, 50 mM acetic acid polybuffer; SID buffer, 33 mM succinic acid, 44 mM imidazole, and 44 mM diethanolamine. This enzyme is a homotetramer, when a single residue is mentioned; all four related residues are implied.

10.1021/bi050881s CCC: $30.25
Published on Web 08/25/2005

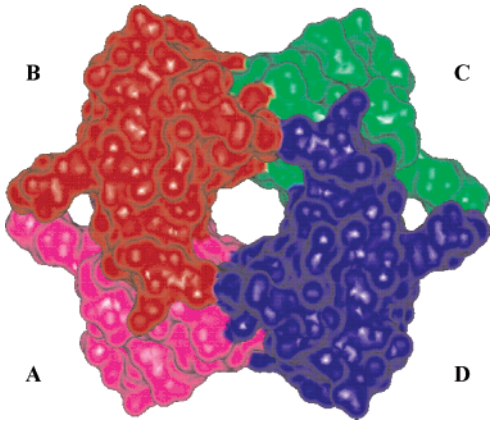

FIGURE 1: A Connolly surface of the R67 DHFR structure. The monomers are labeled A−D and are shown in different colors. The hole in the center of the structure corresponds to the active site pore. The tetramer is a dimer of dimers. The monomer−monomer pairs are colored magenta and red (left side of image) and green and blue (right side of image). The dimer−dimer interfaces occur between the red and green (or magenta and blue) subunits.

shown in Figure 1, the homotetramer possesses 222 symmetry, and a single active site pore (25 Å long) traverses the length of the enzyme.

The symmetry associated with the structure results in multiple (up to four) binding sites for cofactor and substrate. However, time-resolved fluorescence anisotropy and isothermal titration calorimetry (ITC) studies have shown that only two molecules bind concurrently in the active site (*6*). The permutations include two nonproductive homoligand complexes (either two DHF or two NADPH molecules bind) or a productive ternary complex. For the latter, NADPH prefers to bind first, followed by DHF binding to the other half of the pore. Thus R67 DHFR appears to overcome the dilemma posed by its 222 symmetry by using a promiscuous surface that accommodates numerous, different interactions during binding of its two dissimilar ligands.

A model of the two folate complex comes from the 1VIF cocrystal structure; however, this is limited to a description of the pteridine ring positions as electron density is not observed for the *p*-aminobenzoylglutamate tails (*4*). A description of the R67 DHFR·$(NADPH)_2$ complex is not available; however, the nicotinamide rings must lie near each other as a transhydrogenase reaction has been noted between bound reduced acetylpyridine adenine dinucleotide phosphate and $NADP^+$ (*7*). Information concerning the ternary complex comes from interligand NOEs monitoring bound $NADP^+$ and folate, consistent with overlap of the nicotinamide ring of the cofactor and the pteridine ring of folate (*8*). In addition, docking of nicotinamide mononucleotide phosphate (NMNH) into R67 DHFR·Fol I (folate molecule 1 in 1VIF) using DOCK (*9*−*11*) predicts stacking of the reactive rings near the center of the active site pore (*12*). This orientation is consistent with use of an *endo* transition state geometry. In contrast, the *Escherichia coli* chromosomal DHFR uses an *exo* transition state geometry (*13*). The *endo* transition state has been calculated to be ~2 kcal more stable than the *exo* geometry (*13*, *14*).

A site-directed mutagenesis approach to understanding the structure−function relationship in R67 DHFR has identified the K32, Q67, I68, and Y69 residues as having the most effect on binding and catalysis (*15*−*18*). In these studies, mutations affect binding of both NADPH and DHF to similar extents, consistent with residues involved in binding the cofactor also being important in binding substrate.

While a binding mechanism for R67 DHFR has been proposed, a good description of protein−ligand interactions as well as an inventory of ligand−ligand interactions is missing. In this study, we ask: Are any pK_as perturbed during binding? What atoms or groups are important in binding and provide anchoring to the active site? How do multiple interactions contribute to binding and cooperativity? Do the interactions work together to provide an orientation that leads to catalysis? A structure−activity relationship approach was taken to probe how ligand alterations affect both binary (homoligand) and ternary (heteroligand) complex formation. DHFR inhibitors, alternate ligands, and fragments were used to identify regions within the ligand that facilitate binding and determine interligand cooperativity patterns. Isothermal titration calorimetry was used to monitor binding, and for those cases where enthalpic signals were low, ligand solubility was an issue, or ligand availability was limited, K_i studies were performed.

MATERIALS AND METHODS

Protein Purification. R67 DHFR was expressed in *E. coli* SK383 cells in TB media containing 200 μg/mL ampicillin and 20 μg/mL trimethoprim as previously described (*19*). Briefly, ammonium sulfate precipitation and ion-exchange column chromatography were used to purify the protein to homogeneity. Purified samples were dialyzed against distilled, deionized H_2O and then lyophilized. Protein concentrations were determined with a biuret assay (*20*).

Reagents. (A) Cofactor Analogues and Fragments. NADPH was purchased from Alexis Chemicals. NADH, reduced nicotinamide hypoxanthine dinucleotide phosphate (NHDPH), 2′-monophosphoadenosine 5′-diphosphoribose (ATP-ribose; discontinued product), adenosine 5′-diphosphoribose (ADP-ribose), and 2′,5′-diphosphoadenosine (2′,5′-ADP) were obtained from Sigma-Aldrich. The oxidized forms of acetylpyridine adenine dinucleotide phosphate ($AcPADP^+$), thio-$NADP^+$, and NMN^+ were purchased from Sigma-Aldrich. The corresponding reduced forms of these last three compounds were generated using a 10-fold molar excess of $NaCNBH_3$ in 2−5 mL of Tris·HCl (80 mM, pH 8.8) for 24 h at room temperature (4 h for NMN^+) (*7*, *21*). The progress of the reaction was monitored by an increasing absorbance at 340 nm. After reaction, 10 mM imidazole (pH 7.5) was added to dilute the Tris concentration to 5−10 mM. Separation of the reduced species from any unreacted, oxidized form used a 15 × 1.2 cm DEAE-fractogel (Supelco Toyopearl 650M) column equilibrated in the imidazole buffer. The sample was eluted with a 0−0.5 M KCl gradient in the same buffer (0−0.2 M for separation of NMN^+/NMNH). Buffer and salt were removed with an 85 × 1.5 cm P-2 column (Bio-Rad) equilibrated in 10 mM NH_4CO_2 buffer at pH 7.5. Reduced compounds were lyophilized prior to use and kept in the dark whenever possible.

Ligand concentrations were determined spectroscopically using the following extinction coefficients: 6230 L mol^{-1} cm^{-1} at 340 nm for NADPH and NADH (*22*); 6220 L mol^{-1} cm^{-1} at 340 nm for NHDPH (*23*); 5720 L mol^{-1} cm^{-1} at 338 nm for NMNH (*24*); 9100 L mol^{-1} cm^{-1} at 363 nm for

AcPADPH (*25*); 15300 L mol^{-1} cm^{-1} at 259 nm for ATP-ribose (*26*); 11300 L mol^{-1} cm^{-1} at 400 nm for thio-NADPH (*25*).

(B) Substrate Analogues and Fragments. Folate, methotrexate, and aminopterin were purchased from Sigma-Aldrich. Biopterin, 10-methylfolate, 10-formylfolate, pteroyldi-γ-L-glutamate (PG2), pteroylpenta-γ-L-glutamate (PG5), sepiapterin, 5,6,7,8-tetrahydrofolate, and 7,8-dihydrobiopterin were purchased from Schircks Laboratories. 7,8-Dihydrofolate was obtained by the chemical reduction of folate as previously described (*27*). Pteroic acid was purchased from Schircks and reduced to 7,8-dihydropteroic acid (DHP) according to Prabhu et al. (*28*). NMR analysis confirmed formation of the reduced species and the simultaneous disappearance of the oxidized compound. 2-Deamino-2-methyl-5,8-dideazafolate (DMDDF) was synthesized according to Li et al. (*8*). The synthesis of 2-aza-2-deamino-N^{10}-methyl-5,8-dideazafolic acid (ADMDF), N^{α}-(5-deazapteroyl)-L-homocysteic acid (N5DHC), D,L-2-[*N*-(5-deazapteroyl)amino]-4-phosphobutanoic acid (N5DAPB), (6*R*,6*S*)-N^{α}-(5-deaza-5,6,7,8-tetrahydropteroyl)-L-homocysteic acid (THFAC), (6*R*,6*S*)-5,8,10-trideaza-5,6,7,8-tetrahydropteroyl-L-glutamic acid (TDTHF), (2*S*)-2-[5-[*N*-(2-amino-4(3*H*)-oxopyrido-[2,3-*d*]pyrimidin-6-yl)methylamino]-2,3-dihydro-1(3*H*)-oxoisoindol-2-yl]aminopentane-1,5-dioic acid (PT648), and N^{α}-pteroyl-L-ornithine (PT489) were previously described (*29*−*33*). N^{α}-Pteroyl-L-histidine was synthesized as per Mao et al. (*34*).

Ligand concentrations were determined using the following extinction coefficients: 8600 L mol^{-1} cm^{-1} at 370 nm (pH 13) for aminopterin (*35*); 21000 L mol^{-1} cm^{-1} at 291 nm for DMDDF (*8*); 25600 L mol^{-1} cm^{-1} (pH 7) at 263 nm for 10-formylfolate (*36*); 31200 L mol^{-1} cm^{-1} (pH 7) at 290 nm for 5-methyl-5,6-dihydrofolic acid (*36*); 24900 L mol^{-1} cm^{-1} (pH 7) at 280 nm for 10-methylfolate (*36*); 29100 L mol^{-1} cm^{-1} at 297 nm (pH 7) for tetrahydrofolate (THF) (*35*); 27000 L mol^{-1} cm^{-1} at 297 nm (pH 7) for folate (*37*) as well as for pteroyldi-γ-L-glutamate and pteroylpenta-γ-L-glutamate (*38*); 6200 L mol^{-1} cm^{-1} at 330 nm (pH 6.8) for dihydrobiopterin (*39*); 21100 L mol^{-1} cm^{-1} at 254 nm (pH 13) for biopterin (*35*); 10400 L mol^{-1} cm^{-1} at 281 nm (pH 1) for sepiapterin (*39*); 22000 L mol^{-1} cm^{-1} at 278 nm (0.1 N NaOH) for dihydropteroic acid (*40*); 8800 L mol^{-1} cm^{-1} at 365 nm (0.1 N NaOH) for pteroic acid (*36*); 7100 L mol^{-1} cm^{-1} at 370 nm (pH 13) for methotrexate (*41*); 24800 L mol^{-1} cm^{-1} at 277 nm (pH 7.4) for N5DAPB (*33*); 23900 L mol^{-1} cm^{-1} at 293 nm (pH 7.4) for N5DHC (*33*); 21200 L mol^{-1} cm^{-1} at 273 nm (pH 7.4) for THFAC (*33*); 24300 L mol^{-1} cm^{-1} at 293 nm (pH 7.4) for ADMDF (*30*); 21700 L mol^{-1} cm^{-1} at 237 nm (0.1 N NaOH) for TDTHF (*31*); 24900 L mol^{-1} cm^{-1} at 284 nm (0.1 N NaOH) for PT489 (*29*); 20400 L mol^{-1} cm^{-1} at 297 nm (0.1 N NaOH) for PT648 (*32*). The N^{α}-pteroyl-L-histidine concentration was determined using the same λ_{max} and extinction coefficient as for folate.

Isothermal Titration Calorimetry. Affinities and stoichiometries as well as ΔH values were determined for binding of substrate and cofactor analogues using isothermal titration calorimetry (ITC) as previously described (*6*). Measurements were performed on a VP-ITC microcalorimeter from MicroCal interfaced to a Gateway PC for data acquisition and analysis. Origin version 5 scientific software was used to analyze the data. The design and use of this instrument have been previously described (*42*). R67 DHFR concentrations typically ranged between 100 to 150 μM in MTA buffer (50 mM MES, 100 mM Tris·HCl, 50 mM acetic acid, pH 8). Binary complex formation was monitored at 28 °C and involved titration of ligand into the sample cell containing R67 DHFR. Ternary complex formation experiments were carried out at 13 °C to minimize catalysis and typically involved titration of folate analogues into the sample cell, which contained a 1:1 ratio of R67 DHFR to cofactor. When folate was titrated into a mixture of R67 DHFR and the alternate cofactor, NADH, the protein:ligand ratio used was 1:3. Experiments were performed at least in duplicate. Also, a reference titration(s) was performed where ligand was titrated into buffer alone. Buffers used for ITC were filtered and degassed prior to use. The pH values of the protein and ligand solutions were checked and adjusted prior to each set of experiments using aliquots of the same buffer having a pH of 4 or 12. The pH of the solutions was also adjusted at the approximate experimental temperature.

In ITC, the enthalpic signal describes all of the components involved in the binding process, including any effects associated with proton release (or uptake). To determine whether proton release/uptake occurs, binding is performed in various buffers, which possess different heats of ionization. If no proton release/uptake occurs, the observed enthalpy value remains constant. However, if binding is coupled to perturbation of a pK_a, such that proton release/uptake occurs, then the observed enthalpy signal varies on the basis of the equation:

$$\Delta H_{obsd} = \Delta H_{binding} + n\Delta H_{ionization} \quad (1)$$

where ΔH_{obsd} is the observed enthalpy change upon ligand binding to enzyme, $\Delta H_{ionization}$ is the ionization enthalpy of the buffer (same pH and temperature), and n is the number of protons transferred upon ligand binding (*43*). Therefore, several ITC titrations were performed using alternate buffers. The buffers used were 37 mM K_2HPO_4 and 100 mM HEPES with 62 mM NaCl and a polybuffer consisting of 33 mM succinic acid, 44 mM imidazole, and 44 mM diethanolamine (SID) (*44*). The same pH and ionic strength (μ) were maintained as for the MTA buffer (pH 8.0, $\mu = 0.1$). Heats of ionization of the buffers were determined in separate ITC experiments as per Jelesarov and Bosshard (*45*). Briefly, a 5 mM solution of HCl was titrated into the sample cell, which contained buffer. Five to six injections (5 μL) allowed measurement of an average enthalpy change (first injection not included). A control titration was performed by titrating distilled, deionized H_2O into buffer to correct for the heat of dilution. The following enthalpy changes were measured at 13 °C: MTA, −10.1 ± 0.2 kcal/mol; SID, −8.13 ± 0.01 kcal/mol; HEPES with NaCl, −4.45 ± 0.01 kcal/mol; and K_2HPO_4, −1.56 ± 0.02 kcal/mol at pH 8 and −2.4 ± 0.07 at pH 9.0.

Inhibition Kinetics. For those analogues that either had solubility problems or did not produce an enthalpic signal in the ITC, K_i values were determined using either a λ3A or a λ35 spectrophotometer from Perkin-Elmer interfaced with a PC. Briefly, assays were performed at 30 °C in MTA polybuffer at pH 7 (*44*). Substrate (DHF) and cofactor (NADPH) were added, followed by enzyme. In these assays,

NADPH was held at a saturating concentration (100 μM) and the DHF concentration was varied. Five to six different DHF concentrations were used to bracket the DHF K_m value. Inhibition data were then collected by repeating this process and using four to five concentrations of the inhibitor that bracketed the K_i value. Data were collected at least in duplicate. Kinetic rate data were initially graphed using a Lineweaver−Burk plot to assess the type of inhibition present. All inhibitors were competitive, and the K_i was then estimated by plotting the slope of each line in a Lineweaver−Burk plot versus the inhibitor concentration (*46*). Reported K_i values were obtained using a nonlinear, global fit of all the data in SAS using the Michaelis−Menten equation describing competitive inhibition (*47*). The macro for use in SAS is available on the Internet at http://animalscience.ag.utk.edu/faculty/saxton/software.htm.

Docking. DOCK version 4.0 was used to identify potential ligands for R67 DHFR. This program uses van der Waals interactions in its scoring and allows ligand flexibility (*9*−*11*). The DOCK suite of programs was used to create a reverse image of the active site described by sphere clusters, where each point is a putative atom position for docked ligands. A sphere cluster was generated for the apoenzyme with all waters removed. A grid surface was calculated for the protein using a Lennard-Jones 6-12 potential and a dielectric ratio of 4. Initial docking of a subset of compounds from the Cambridge Structural Database (1998) used a shape scoring function and a simultaneous search where all torsions are searched and minimized concurrently. After identification of a series of potential ligands, anchor searching was then used where docking of a rigid, anchor fragment is performed first, followed by stepwise rebuilding and docking of the rest of the molecule. High scoring molecules were then evaluated on the basis of commercial availability as well as obvious inhibition of R67 DHFR activity.

RESULTS

Previous studies have found that two NADPH molecules bind to R67 DHFR, with negative cooperativity. In contrast, two folate (or DHF) molecules bind with positive cooperativity. Formation of a ternary complex upon addition of folate to a 1:1 mixture of R67 DHFR·NADPH utilizes the positive cooperativity between cofactor and substrate (*6*). These patterns funnel binding toward the productive NADPH·DHF complex and indicate that interligand cooperativity is an important component in R67 DHFR function. ITC and steady-state kinetics, utilizing variants and/or fragments of NADPH and DHF (see Figure 2), were used to investigate the nature of ligand binding and interligand cooperativity patterns within the R-plasmid-encoded DHFR.

Isothermal Titration Calorimetry Studies. (A) Binary Complex Formation Using Cofactor Analogues and Fragments. The titration of reduced nicotinamide hypoxanthine dinucleotide phosphate (NHDPH) into R67 DHFR is shown in Figure 3. The ITC data for the NADPH analogues were initially fit to a model of sequential binding sites. In this model, the stoichiometry must be provided and was set equal to 2. However, as the cofactor species were varied, often the data were better fit by a single-site (or set of sites) model. For these cases, the "*c* value" ($=[P_{total}]/K_d$) for the second site was beyond the suggested range (1−1000), indicating weak binding and difficulty in determining this K_d with low error (*42*). Thus data for NADH, reduced acetylpyridine adenine dinucleotide phosphate (AcPADPH), and NADPH fragments were fit to a single-site model. The K_d values, binding stoichiometries, and ΔH values associated with binding of the various compounds are given in Table 1.

Binding of NADPH analogues was generally found to be highly variable. NHDPH bound similarly to NADPH. Substitution of a sulfur atom into the carboxamide moiety of the nicotinamide ring (thio-NADPH) weakens binding of the first molecule by ~3-fold. A different modification of the carboxamide group in reduced acetylpyridine adenine dinucleotide phosphate (AcPADPH) weakens K_{d1} 33-fold. These analogues indicate that the carboxamide group is strongly involved in binding to the protein. Loss of the charged phosphate group at the 2′ position of the adenine ribose of NADH weakens binding affinity by ~14-fold and supports a role for the phosphate in binding (*16*, *18*, *48*). Titration of the oxidized species, thio-$NADP^+$ and Ac-$PADP^+$, showed weak ITC signals and no evidence of saturation indicating the oxidized species bind more weakly than the reduced species. Preferential binding of the reduced species has also been seen for the NADPH and $NADP^+$ pair (*6*).

Not surprisingly, fragmentation of the cofactor reduces binding affinity. The shapes of the binding curves for the NADPH fragments were hyperbolic rather than sigmoidal, consistent with a better fit of the data to a single-site or set of sites model. Loss of the nicotinamide ring (in ATP-ribose) weakens binding 64-fold compared to NADPH. The additional loss of phosphate and sugar groups in ADP-ribose and 2′,5′-diphosphoadenosine weakens binding 110- and 250-fold when compared to NADPH. The enthalpic signal also gradually diminishes, with binding of 2′,5′-diphosphoadenosine being entropically driven. These trends are shown in Figure 3C by plots of Q_{total} (total heat) for this series of titrations. Titration of NMNH into R67 DHFR was performed, but no enthalpic signal was observed (using a syringe concentration of 2.7 mM).

(B) Binary Complex Formation Using Substrate Analogues and Fragments. The titration of 2-deamino-2-methyl-5,8-dideazafolate (DMDDF) into R67 DHFR is shown as a supplemental figure (see Supporting Information). In general, the analogues of folate that displayed an ITC signal exhibited positive cooperativity. This phenomenon has been observed previously, and a "hook" appears in the titration (*6*). Data fitting used a sequential sites model. No cooperativity was observed in binding of the *p*-aminobenzoylglutamate tail of folate (pABA-Glu), and these data were fit to a single-site (or set of sites) model.

Table 2 lists the results of ITC titrations for binding of folate analogues and the pABA-Glu tail to R67 DHFR. For binding of aminopterin, substitution of O4 in folate by an amine group does not greatly alter binding. From the DMDDF titrations, the 2-deamino-2-methyl substitution as well as the substitution of N5 and N8 by carbon reduces the K_d values by 4−7-fold, when compared to folate binding.

To explore the role of the glutamate tail in folate binding, polyglutamylated folate was used as a ligand. Increasing the number of glutamic acids to two or five with the use of pteroyldi-γ-L-glutamate and pteroylpenta-γ-L-glutamate had minimal effects as K_d values changed by less than 2-fold.

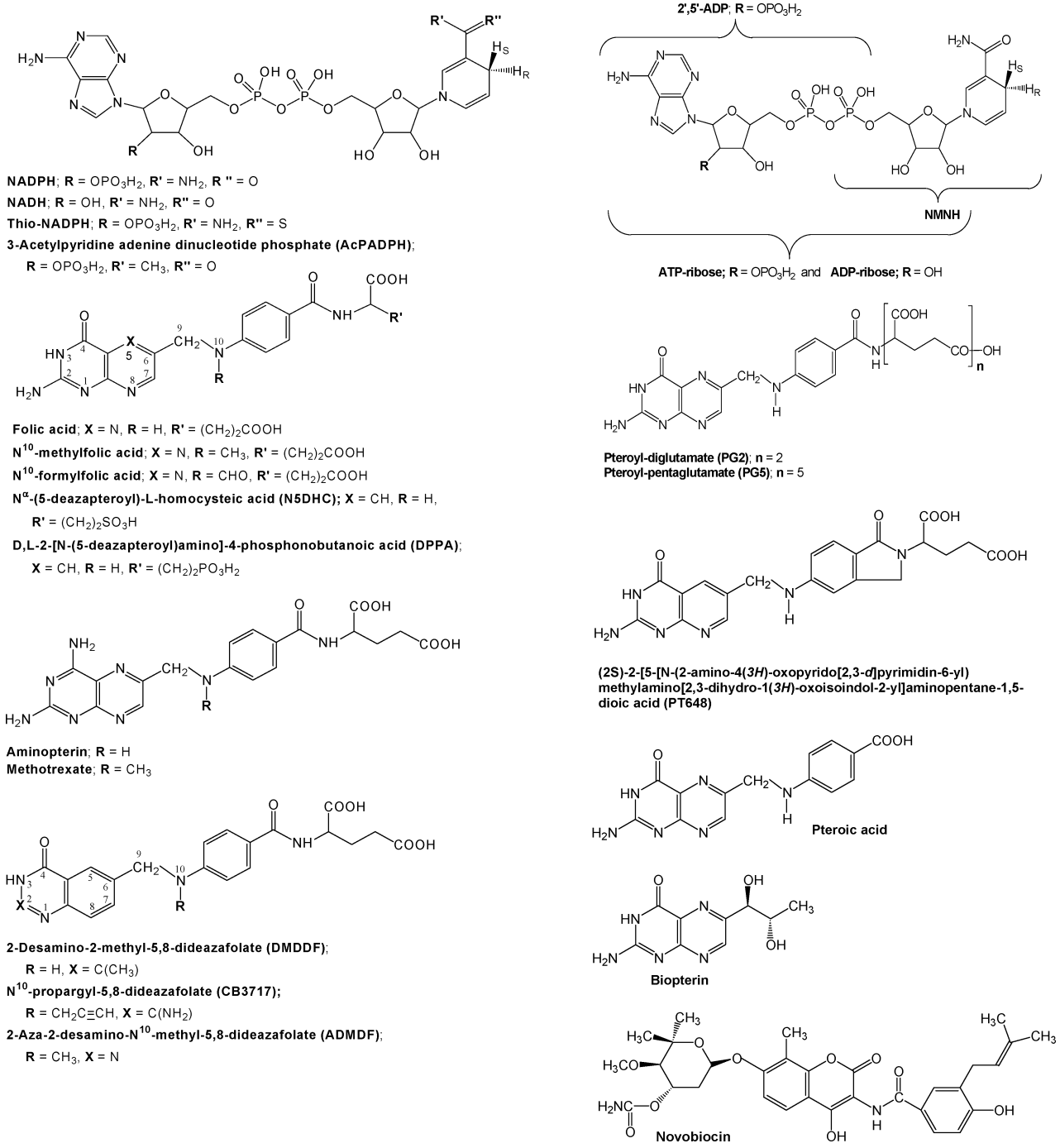

FIGURE 2: Structures of the various ligands used in the binding studies. 7,8-Dihydrofolate, 7,8-dihydropteroic acid, and 7,8-dihydrobiopterin are reduced across the C7−N8 bond. 5,6,7,8-Tetrahydrofolate and its analogues are also reduced across the N5−C6 bond. In sepiapterin, the CHOH−CHOH−CH_3 side chain of biopterin is replaced by CO−CHOH−CH_3. N^{α}-pteroyl-L-histidine and N^{α}-pteroyl-L-ornithine replace glutamate in the tail by histidine and ornithine, respectively. The acids are drawn in their un-ionized forms, as they were originally named. In NHDPH, adenine is replaced by hypoxanthine where the exocyclic NH_2 is substituted by an oxygen.

Addition of pABA-Glu as a ligand results in greatly weakened binding but an observable enthalpy change.

Binding of other folate analogues under binary complex conditions was explored by ITC with limited success. While methotrexate (MTX) clearly bound, a weaker interaction occurred, as saturation was not reached up to a 25:1 molar ratio of ligand to protein. Also, an obvious titration occurred with 2-aza-2-deamino-N^{10}-methyl-5,8-dideazafolate (ADMDF) but was difficult to fit without constraints on the stoichiometry and ΔH. A clear titration was observed using dihydropteroate; however, saturation was not reached, probably due to weaker binding and/or a more limited solubility (syringe concentration of 2.6 mM). Unlike these analogues, no discernible titrations were observed for 10-methylfolate, 10-formylfolate, dihydrobiopterin, or (6*R* or 6*S*)-5-methyl-5,6-dihydrofolic acid.

Finally, use of DOCK to identify alternate ligands that might bind R67 DHFR identified novobiocin as a candidate. Novobiocin is an aminocoumarin drug that inhibits bacterial type II topoisomerase DNA gyrase by competitively binding to its ATP site (*49*, *50*); its structure is given in Figure 2. Using an ITC approach, novobiocin was found to bind with

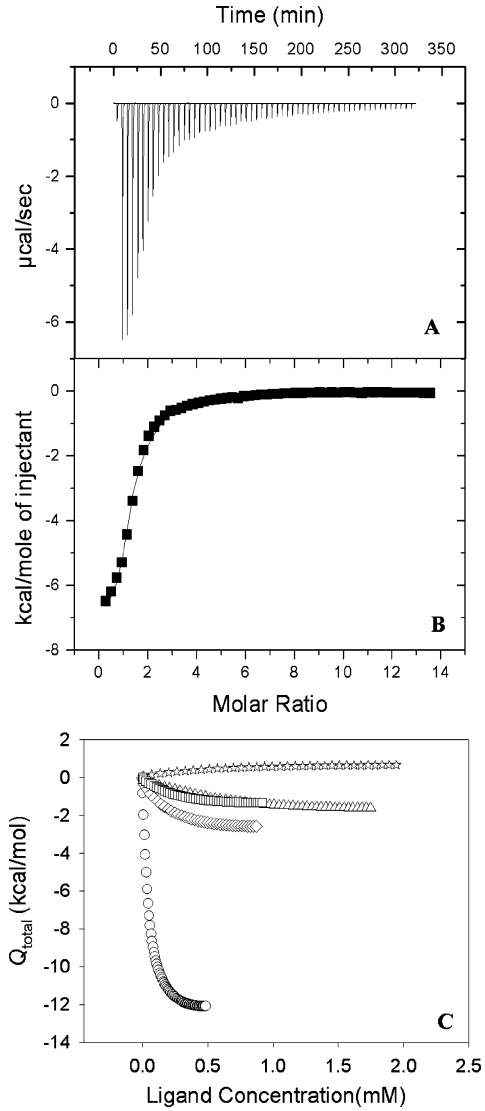

FIGURE 3: Titration of NADPH analogues into R67 DHFR as monitored by ITC. Panel A shows the series of peaks generated from the heat liberated upon binding of NHDPH as monitored by ITC. As the protein approaches saturation, less of each subsequent addition is bound, so the peaks decrease in height. The protein concentration was 103 μM tetramer. Panel B shows the heat liberated per mole of titrant vs the cofactor:protein tetramer molar ratio. The smooth line shows the fit of the data to a two interacting site model displaying negative cooperativity. Best fit values for K_d and ΔH values are given in Table 1. Note: due to mixing artifacts, the heat associated with the first peak in panel A was not included in panel B or in the data analysis. Panel C shows the Q_{total} (total heat) titrations associated with several NADPH-based ligands. Data for NADPH, AcPADPH, ATP-ribose, ADP-ribose, and 2′,5′-diphosphoadenosine are represented by ○, ◇, □, △, and ☆, respectively.

a K_d of 120 ± 5.0 μM, a ΔH of −13000 ± 360 kcal/mol, and a stoichiometry of 1.8 ± 0.1.

(C) Ternary Complex Formation. The above experiments probed the determinants involved in formation of the nonproductive, homoligand complexes. In the studies described below, the importance of ligand atoms in formation of heteroligand complexes such as the substrate·cofactor pair was monitored. As folate is a poor substrate for R67 DHFR, the question arises whether minimal reduction could occur during some of these titrations. Our previous studies found k_{cat} for folate reduction at pH 8 (20 °C) to be 0.0036 min^{-1} (*6*). As the ITC titrations take 2−3 h, this low rate could still contribute to some minimal level of catalysis. Thus, additional studies were performed, and two control points done within 5 min of each other at folate concentrations of 1 and 200 μM were found to display the same relative position on the titration curve as seen in the longer 2−3 h data set (*6*). This observation indicates that any contribution of catalysis to the binding curve in R67 DHFR is minimal. As a further precaution, titrations were done at 13 °C to minimize catalysis.

The titration of pteroyldi-γ-L-glutamate (PG2) into a 1:1 mixture of R67 DHFR·NADPH is shown as a supplemental figure (see Supporting Information). As K_{d1} for NADPH is 2.5 μM, the main species expected in the calorimeter cell is R67 DHFR·NADPH when ∼100 μM concentrations of both species are present. Addition of PG2 results in formation of the R67 DHFR·NADPH·PG2 complex. A single-site model was used in fitting, and Table 3 lists the values obtained in fitting.

When alternate cofactors are used to form the ternary complex, the largest changes in K_d (7-fold) occur in the presence of thio-NADPH. Only 4-fold changes in K_d are observed using NADH.

When folate analogues are titrated into R67 DHFR·NADPH, the largest K_d changes (14-fold) occur using 10-formylfolate, suggesting that increasing the size of the group off N10 weakens binding. Use of 10-methylfolate has an intermediate effect. Addition of one to four additional glutamates to the folate tail does not alter the K_d associated with ternary complex formation. Use of DMDDF shows ∼10-fold tighter binding to the R67 DHFR·NADPH complex while binding of ADMDF does not show a significant change with respect to binding of folate.

Binding of fragments lacking the glutamate tail was also tested using ITC. While titration with pteroic acid (339 μM syringe concentration) did not show a signal, use of the reduced species, dihydropteroate (DHP), did. [DHP is a very poor substrate and minimal catalysis occurs under these conditions (S. Chopra, unpublished results).] These different results are likely due to weaker binding of pteroic acid (see K_i studies below) coupled with a lower concentration of the ligand in the syringe due to a more limited solubility. While the glutamate tail is removed in DHP, a negative charge still remains, albeit in a different position. Thus it is surprising that binding is weakened only 5-fold [compared to the K_d value describing binding of DHF to R67 DHFR·NADP$^+$ (*6*)] and a reasonable enthalpy change is observed.

Binding of dihydrobiopterin lacking the pABA-Glu tail was also tested, and no isotherm was observed. Either it does not bind (tested by K_i studies; see below) or a charged tail provides most of the enthalpic signal associated with binding. As the syringe concentration was 3.2 mM for dihydrobiopterin, there does not seem to be a solubility problem.

Binding of other folate analogues to form the ternary complex was explored by ITC; however, aminopterin (up to 7 mM) and MTX (up to 19 mM) do not appear to form a ternary complex. These results indicate a large role for O4 in folate/DHF in binding to R67 DHFR·NADPH.

Is Binding Coupled to Any Protonation Events? The active site pore of R67 DHFR is large and accessible to solvent (*4*, *5*, *12*); thus it was not clear whether any pK_as would be perturbed. To examine whether binding is accompanied by

Table 1: Dissociation Constants and Heats of Enthalpy for Binding of Cofactor Analogues or Fragments to R67 DHFR in MTA Buffer, pH 8.0[a]

ligand	dissociation constant (μM)	ΔH_{obsd} (cal/mol)	stoichiometry
NADPH[a]	K_{d1} 2.5 ± 0.2	−8600 ± 200	1.6 ± 0.14[b]
	K_{d2} 96 ± 4.0	−5800 ± 2500	
nicotinamide hypoxanthine dinucleotide phosphate, reduced (NHDPH)	K_{d1} 2.0 ± 0.4	−6700 ± 110	2[c]
	K_{d2} 46 ± 4.9	−4200 ± 150	
thio-NADPH	K_{d1} 7.2 ± 0.4	−6900 ± 40	2[c]
	K_{d2} 78 ± 2.0	−6700 ± 100	
nicotinamide adenine dinucleotide (NADH)	K_{d1} 34 ± 0.7	−11000 ± 100	1.1 ± 0.01[d]
3-acetylpyridine adenine dinucleotide phosphate, reduced (AcPADPH)	K_{d1} 83 ± 4.0	−2400 ± 80	0.94 ± 0.05[d]
2′-monophosphoadenosine 5′-diphosphoribose (ATP-ribose)	K_{d1} 160 ± 6.0	−1700 ± 46	1.2 ± 0.028[d]
adenosine 5′-diphosphoribose (ADP-ribose)	K_{d1} 280 ± 25	−1000 ± 59	1.6 ± 0.12[d]
2′,5′-diphosphoadenosine	K_{d1} 620 ± 93	+560 ± 180	2.1 ± 0.62[d]

[a] Macroscopic K_d values are reported. The relationship between microscopic binding constants and macroscopic values is $K_{macro} = k_{micro}/2$ and $K_{macro} = 2k_{micro}$ for the first and second binding events, respectively. [b] From Bradrick et al. (*6*). [c] Data fit to an interacting sites model, stoichiometry set equal to 2. [d] Data fit to a single-site (or set of sites) model.

Table 2: Dissociation Constants and Heats of Enthalpy for Binding of Substrate Analogues and Fragments to R67 DHFR in MTA Buffer, pH 8.0[a]

ligand	dissociation constant (μM)	ΔH_{obsd} (cal/mol)	stoichiometry
folate	K_{d1} 120 ± 15	−1600 ± 270	2
	K_{d2} 36 ± 3.6	−13000 ± 270	
aminopterin	K_{d1} 240 ± 11	−5100 ± 90	2
	K_{d2} 35 ± 1.1	−9200 ± 95	
2-deamino-2-methyl-5,8-dideazafolate (DMDDF)	K_{d1} 460 ± 44	−4000 ± 360	2
	K_{d2} 5.3 ± 0.47	−11000 ± 330	
5,8-dideaza-10-propargylfolate (CB3717)[b]	K_d 2.2 ± 0.2	−14500 ±1500	2
pteroyldi-γ-L-glutamate	K_{d1} 76 ± 4.4	−3600 ± 30	2
	K_{d2} 43 ± 1.4	−6900 ± 40	
pteroylpenta-γ-L-glutamate	K_{d1} 170 ± 9.4	−3400 ± 90	2
	K_{d2} 55 ± 1.9	−9400 ± 110	
p-aminobenzoylglutamate	K_d 2000 ± 390	−100 ± 32	3.9 ± 1.4

[a] Macroscopic K_d values are reported. [b] From Bradrick et al. (*6*).

Table 3: Dissociation Constants and Heats of Enthalpy for Binding of Substrate Analogues to R67 DHFR·Cofactor in MTA Buffer, pH 8.0, 13 °C[a]

titration (ligand in syringe into cuvette solution)	dissociation constant (μM)	ΔH_{obsd} (cal/mol)	stoichiometry
DHF into R67 DHFR·$NADP^+$	4.8 ± 1.0	−11700 ± 300	1.22 ± 0.01[b,c]
folate into R67 DHFR·NADPH	11 ± 0.4	−8500 ± 500	0.87 ± 0.01[b]
folate into R67 DHFR·NADH	40 ± 1.4	−3900 ± 73	0.90 ± 0.02
folate into R67 DHFR·thio-NADPH	77 ± 3.0	−13000 ± 600	0.57 ± 0.06
folate into R67 DHFR·AcPADPH	10 ± 0.3	−12000 ± 100	0.69 ± 0.01
10-methylfolate into R67 DHFR·NADPH	45 ± 0.9	−6200 ± 65	0.8 ± 0.01
10-formylfolate into R67 DHFR·NADPH	150 ± 5	−1300 ± 33	1.4 ± 0.02
dihydropteroic acid into R67 DHFR·NADPH	25 ± 0.4	−6900 ± 50	1.1 ± 0.01
pteroyldi-γ-L-glutamate into R67 DHFR·NADPH	17 ± 0.4	−6600 ± 30	0.9 ± 0.005
pteroylpenta-γ-L-glutamate into R67 DHFR·NADPH	16 ± 0.2	−9200 ± 39	0.8 ± 0.004
2-deamino-2-methyl-5,8-dideazafolate into R67 DHFR·NADPH	1.3 ± 0.1	−7000 ± 27	1.2 ± 0.003
2-aza-2-deamino-N^{10}-methyl-5,8-dideazafolic acid into R67 DHFR·NADPH	14 ± 0.4	−7800 ± 60	1.0 ± 0.007

[a] The ratio of cofactor to enzyme was 1:1 except for NADH where the ratio was 3:1. [b] From Bradrick et al. (*6*). [c] Titration at 28 °C.

protonation, formation of the two NADPH, two folate, and the NADPH·folate or the $NADP^+$·DHF complexes was monitored in various buffers possessing different heats of ionization. No differences in ΔH associated with formation of either the two NADPH complex or the R67 DHFR·$NADP^+$·DHF complex were observed in K_2HPO_4 and MTA buffers. However, the enthalpy change associated with binding of folate to form either the two folate or the folate·NADPH complex *was* found to vary with different buffers. Using eq 1, a plot of ΔH_{obsd} versus the buffer heat of ionization is linear, and the slope yields the number of protons taken up or released upon binding. The *y*-intercept gives the ΔH associated with binding describing van der Waals, H-bonds, ionic interactions, etc. as well as a term describing the ΔH associated with protonation (*45*). Figure 4 shows the plot associated with binding of folate to R67 DHFR·NADPH at pH 8.0. The slope is 0.4 ± 0.05, and the $\Delta H_{binding}$ value is −13.1 kcal/mol. The slope indicates that protons are taken up upon binding (*51*).

Buffer-dependent alteration in ΔH_{obsd} values could arise from titrations in either the enzyme or ligand upon binding. As buffer-dependent ΔH values were not observed for binding of DHF in forming the $NADP^+$·DHF complex, it seems likely that a pK_a difference between folate and DHF is associated with the difference in buffer dependence. From NMR studies by Poe (*52*), a pK_a of 8.38 was observed and identified with titration of the N3 atom in the keto tautomer of folate (*53*). In contrast, a pK_a of 9.54 for this same

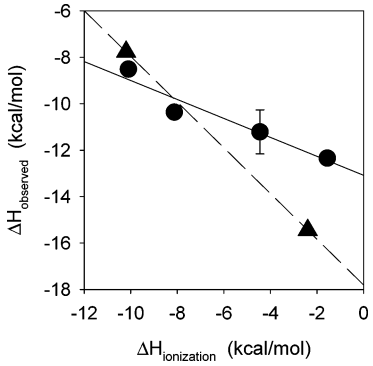

FIGURE 4: Buffer effects associated with folate binding to R67 DHFR·NADPH. The buffers utilized are phosphate, HEPES, SID, and MTA. Data at pH 8 are shown by ● and a solid line. Data at pH 9 are given by ▲ and a dashed line. Errors are smaller than the symbols, except for the HEPES point at pH 8.

protonation was observed for DHF (*52*) or, more recently, a pK_a of 10.8 by a different group (*54*). These observations suggest that DHF binds to R67 DHFR without proton uptake as its N3 pK_a is higher than the pH in the experiment (8.0). In contrast, folate likely binds to R67 DHFR with partial proton uptake as its pK_a is near the pH used in the experiment. In other words, as the slope in Figure 4 is 0.4, 40% of the time, anionic (N3 deprotonated) folate will bind at pH 8.0 accompanied by proton uptake, while 60% of the time, neutral (N3 protonated) folate will bind. To investigate this hypothesis, ITC titrations were also done in MTA and K_2HPO_4 buffers at pH 9.0. At this higher pH, a greater slope of 0.9 ± 0.01 was observed for a plot of ΔH_{obsd} versus $\Delta H_{ionization}$ (Figure 4). Here 90% of the time, binding of N3 deprotonated folate occurs, accompanied by proton uptake. These various observations suggest that the buffer-dependent binding of folate arises from a perturbation of the N3 pK_a when bound to R67 DHFR. The basic (anionic) species will carry a negative charge either at N3 in the keto tautomer or at O4 in the enol tautomer (*53*). This hypothesis is consistent with the crystal structure of the two folate complex (*4*) or the docked structure of the NMNH·folate complex (*12*), where the N3 and O4 atoms occur at the hourglass center of the pore and access to solvent is restricted.

Due to limited availability of other ligands, protonation effects using alternate buffers were only pursued for N^{10}-methylfolate. For this compound, two buffers were used (MTH and K_2HPO_4), and a buffer sensitivity for the enthalpy change was observed. The slope of a ΔH_{obsd} versus the buffer heat of ionization plot was 0.56 ± 0.015 (data not shown). For other ligands, as NADPH addition was not accompanied by buffer-dependent effects, it seems likely that binding of cofactor analogues also would not be affected. Further, a previous study of DHF bound to R67 DHFR found the N5 pK_a to be <5 (*55*), consistent with minimal perturbation of this pK_a [normally ~2.59 (*54*)].

Steady-State Inhibition Kinetics. Inhibition studies were pursued for several reasons. First, K_i studies are an independent approach that allows assessment of binding strength. In general, the K_i values obtained correlate with the K_d values observed by ITC. More importantly, several folate analogues did not display an enthalpic signal in ITC titrations, and K_i determination allows assessment of binding strength for these ligands. Finally, limited solubility and/or availability were (was) an issue for some compounds, and K_i studies only require a few milligrams of sample.

The inhibition of R67 DHFR activity by ADMDF is shown as a supplemental figure (see Supporting Information). All of the compounds tested were competitive inhibitors, and their respective K_i values are listed in Table 4. The first section in the table reports K_i values for fragments of folate/DHF. While an ITC approach did not show an enthalpic signal upon addition of these fragments, they do bind to R67 DHFR. As the fragment size is decreased, binding of oxidized species is weakened up to 8-fold compared to the folate K_i while binding of reduced species is weakened up to 33-fold compared to the DHF ternary complex K_d value (*6*).

The next section of the table investigates the effect of alternate tails on folate binding. Addition of one to four glutamates (in PG2 and PG5) has a minimal effect. When binding of N^{α}-pteroyl-L-histidine or N^{α}-pteroyl-L-ornithine is explored, slightly weaker binding (<2-fold) is observed, suggesting a tolerance for amino acid side chain substitution in the tail. Substitution of the glutamate tail by 4-phosphonobutanoic acid also has a minimal effect (N5DAPB also contains a 5-deaza substitution). The weakest binding involves PT648, an N5-deaza analogue containing a rotationally restricted glutamate tail, where the K_i is increased 3-fold. The lowest K_i (6-fold smaller than for folate) describes binding of N5DHC where the glutamate tail is replaced by homocysteic acid. This compound also has an N5-deaza substitution and is quite similar to N5DAPB, so it is surprising that it displays tighter binding. Perhaps the single (L) isomer for N5DHC (vs a mixture of D,L isomers for N5DAPB) binds more tightly.

The last section of the table contains miscellaneous compounds. Introduction of a 10-methyl group into folate results in 3-fold weaker inhibition. While DMDDF binds 5-fold more tightly than folate, numerous substitutions are present, making interpretation of the basis of tighter binding difficult. ADMDF also has numerous changes in the pteridine ring, yet binding is not greatly altered, suggesting a large tolerance for substitutions at N5, at C2, and on the C2 amino group or, alternatively, a set of positive and negative effects that cancel out. Alterations could include increased lipophilicity of the compounds, altered N3 pK_a values, changed electronic structure of the ring (pteridine to quinazoline), and loss of potential H-bond acceptors/donors at N5, N8, and NA2.

A further observation is that the reduction state of the compound affects binding, with the dihydro form interacting more tightly than the fully oxidized form. This can be seen by comparing folate vs DHF binding as well as pteroic acid vs DHP binding. Further, those compounds that are based on the tetrahydrofolate scaffold show minimal inhibition with K_i values >460 μM. For example, THFAC is identical to N5-DHC except for the reduction state of the pteridine ring, yet there is an ~150-fold difference in K_i values. When 400 μM tetrahydrofolate was tested as an inhibitor, no change in the R67 DHFR reaction rate was observed.

Finally, several compounds showed no inhibition of the R67 DHFR reaction, including aminopterin and MTX (up to 500 μM). 10-Formylfolate also did not inhibit up to a concentration of 380 μM. (6*R* or 6*S*)-5-Methyl-5,6-dihydrofolic acid did not inhibit up to 530 μM.

Table 4: K_i Values for Folate Analogues and Fragments Exhibiting Competitive Inhibition with Respect to DHF

folate analogue/fragment	K_i (μM)
folate	20 ± 0.1[a]
pteroic acid	62 ± 6.4
dihydropteroic acid	27 ± 1.3
sepiapterin	160 ± 15
dihydrobiopterin	160 ± 18
PG5	28 ± 2.1
PG2	26 ± 1.9
N^{α}-pteroyl-L-histidine	37 ± 3.9
N^{α}-pteroyl-L-ornithine	28 ± 2.2
(2*S*)-2-[5-[*N*-(2-amino-4(3*H*)-oxopyrido[2,3-*d*]pyrimidin-6-yl)methylamino]-2,3-dihydro-1(3*H*)-oxoisoindol-2-yl]aminopentane-1,5-dioic acid (PT648)	65 ± 3.4
N^{α}-(5-deazapteroyl)-L-homocysteic acid (N5DHC)	3.1 ± 0.2
D,L-2-[*N*-(5-deazapteroyl)amino]-4-phosphobutanoic acid (N5DAPB)	22 ± 1.1
10-methylfolate	67 ± 7.3
10-formylfolate	>380
2-deamino-2-methyl-5,8-dideazafolate (DMDDF)	4.0 ± 0.4
2-aza-2-deamino-N^{10}-methyl-5,8-dideazafolic acid (ADMDF)	37 ± 1.7
aminopterin	>500
methotrexate (MTX)	>500
(6*R* or 6*S*)-5-methyl-5,6-dihydrofolic acid	>530
tetrahydrofolate (THF)	>400
(6*R*,6*S*)-N^{α}-(5-deaza-5,6,7,8-tetrahydropteroyl)-L-homocysteic acid (THFAC)	>460
(6*R*,6*S*)-5,8,10-trideaza-5,6,7,8-tetrahydropteroyl-L-glutamic acid (TDTHF)	>460

[a] From Bradrick et al. (*6*); refit using SAS (*47*).

Use of NMNH as an Alternate Cofactor. The question of whether NMNH binds to R67 DHFR arises as this ligand did not provide a signal in our ITC experiments. To confirm an earlier report that NMNH serves as an alternate cofactor (*25*), steady-state kinetic analysis was performed where the NMNH concentration was varied in the presence of a saturating DHF concentration. A k_{cat} of 0.13 ± 0.01 s^{-1} and a K_m of 360 ± 50 μM were observed, indicating 120-fold weaker binding and a 10-fold reduction in k_{cat}. These values compare well with those previously reported (*25*).

DISCUSSION

Structure−activity relationships are a companion approach to site-directed mutagenesis studies to address how ligands bind. In our studies, alternate ligands have been used to establish which are the important interactions between R67 DHFR and substrate or cofactor. In addition, as the ITC monitors enthalpic contributions to binding, we can begin to describe which ligand fragments are most important in pairwise interactions.

What Are the Enthalpic Contributions to Binary Complex Binding? Some interesting trends are found in ΔH vs $T\Delta S$ plots describing binding of NADPH and folate analogues/fragments (Figure 5). For folate and its analogues, binding of the second molecule is enthalpy driven (ΔH_2). In contrast, for NADPH and its analogues, the enthalpic contribution for binding of the first molecule displays a more negative value (ΔH_1) than for the second molecule (Table 1). These observations, coupled with the respective K_d values in the binding scheme from Bradrick et al. (*6*), continue to support a preferred binding pathway (NADPH first, followed by folate/DHF), as well as suggesting that it is difficult for a single folate/DHF molecule to bind well, as it prefers an interaction partner (either a second folate/DHF or a previously bound NADPH).

A second observation from Figure 5 is that truncation of ligands results in weaker binding as well as a smaller exothermic signal. For example, in the NADPH series using ATP-ribose, ADP-ribose, and 2′,5′-ADP, the binding affinity

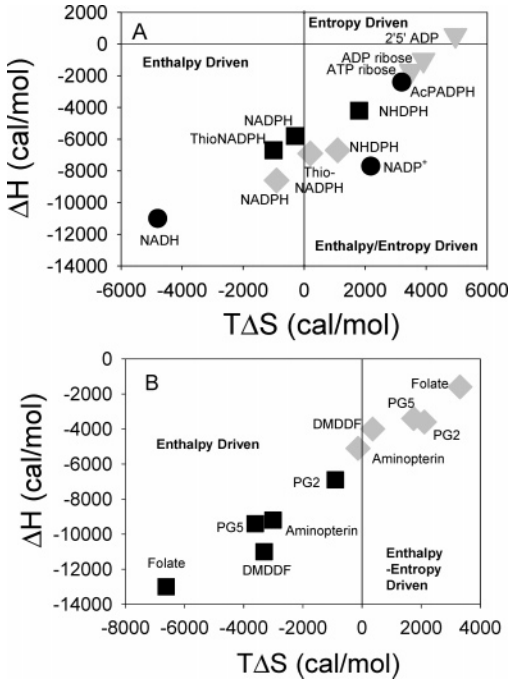

FIGURE 5: Enthalpy−entropy compensation plots for formation of binary complexes. Panel A shows a plot of $T\Delta S$ versus ΔH for binding of various cofactor ligands to R67 DHFR. For those ligands that were fit to an interacting site model, the first binding site is represented by gray filled diamonds and the second site by ■. For those ligands fit to a single-site model, the data are shown as ●. Binding of truncated ligands is given by gray filled upside down triangles. The $NADP^+$ data point comes from Bradrick et al. (*6*). Enthalpy-driven binding occurs in the lower left quadrant, enthalpy/entropy-driven binding in the lower right quadrant, and entropy-driven binding in the upper right quadrant. Panel B shows a plot of $T\Delta S$ versus ΔH describing binding of various substrate ligands to R67 DHFR. All ligands were fit to an interacting site model, and the first binding site is represented by gray filled diamonds and the second site by ■.

is reduced along with the enthalpic contribution to binding (Table 1). These observations underscore the importance of ligand connectivity during binding. Previous studies on connectivity describe how binding and/or catalysis utilizing the entire ligand are (is) more than the sum of its parts (*56*−*58*).

When binding of NADPH is compared with that of ATP-ribose, it is clear that the nicotinamide ring contributes substantially to the binding enthalpy value. Successive truncations to 2,5-diphosphoadenosine further weaken binding. However, when only NMNH is used as a ligand, no enthalpic signal is observed. These separate observations point to multiple interactions as well as to ligand connectivity being important to the overall ΔH and ΔG values.

When AcPADPH binding is compared to that of NADPH, much weaker binding is observed as well as large effects on ΔH. This observation suggests that one of the most important cofactor binding components is the amine in the carboxamide group off the nicotinamide ring.

As previous studies have identified two ionic interactions between NADPH and R67 DHFR (*18*, *48*), binding of NADH was of interest. For NADH, which lacks the 2′-phosphate group, weaker binding is observed; however, it is difficult to compare ΔH values as the data were fit to different models (two sites for NADPH, single site for NADH).

When binary complex formation of DHF/folate analogues is considered, the variation in K_d values is less than 7-fold (see Table 2). However, several of the ligands did not bind or provide an enthalpic signal. As a first example, removal of the pABA-Glu tail (dihydrobiopterin) leads to loss of an ITC signal, suggesting that the pABA-Glu tail provides a large contribution to the enthalpic interactions with the protein. To test whether loss of the ITC signal is due to weaker binding, a second technique, K_i determination, was utilized. When compared to the DHF ternary K_d value, a 33-fold increase in K_i is observed as the negatively charged pABA-Glu tail is removed. Therefore, loss of the ITC signal appears to arise from effects on enthalpy and most likely disruption of some type of ionic interaction ($1/r$ distance relationship) with the symmetry-related K32 residues (*18*, *48*). This hypothesis is supported by the observation that an isotherm for dihydropteroate binary complex formation was clearly observed, although saturation was not obtained. This suggests a correlation between the presence of a negative charge (albeit in a different position in DHP) and the enthalpic signal.

A second surprise is that neither 10-methylfolate nor MTX readily formed a binary complex with R67 DHFR, while aminopterin did. These observations indicate a role for the N10 atom in formation of the two folate complex. This result contrasts with our previous finding that two 5,10-dideaza-10-propargylfolate (CB3717) molecules bind tightly (*6*). Since the active site of R67 DHFR is large and open and possesses an amphipathic surface, one possibility is some variability in how the ligands bind so that varying substituents at N10 as well as N5 and N8 can have nonadditive effects.

What Are the Enthalpic Contributions to Ternary Complex Binding? From eq 1, binding can be coupled with proton uptake or release. Our studies find coupled proton uptake upon folate binding to R67 DHFR·NADPH but not for DHF binding to R67 DHFR·$NADP^+$. An increased proton uptake was found when the ternary folate titrations were performed at pH 9 as compared to pH 8. As discussed above, these observations suggest that as the N3 pK_a for DHF is >9.5 (*52*, *54*), DHF is in the correct ionization state for binding at pH 8. However, as the N3 pK_a for folate is 8.38 (*52*), not all of the folate molecules are in the preferred ionization state; therefore, some coupled proton uptake occurs upon binding. At pH 9, increased proton uptake occurs upon folate binding. This hypothesis indicates a strong preference for an uncharged pteridine ring so that perturbation of the N3 pK_a in folate occurs upon binding to R67 DHFR. Again, this proposal is consistent with the crystal structure of the two folate complex (*4*) as well as the docked structure of the NMNH·folate complex (*12*), where the N3 and O4 atoms are predicted to form H-bonds with the backbone NH and O atoms of I68. These proposed interactions are shown in Figure 6A.

Can protonation effects be invoked to explain the different K_d's for binding of folate, DMDDF, and ADMDF to R67 DHFR; i.e., do the various substitutions in these compounds affect the N3 pK_a and thus the observed K_d at pH 8? The N3 pK_a values for folate, DMDDF, and ADMDF were calculated using the rules of Perrin (*59*) as well as the ACD/I-Lab Web service (see http://www.acdlabs.com/products/phys_chem_lab/pka/batch.html). While the calculated values are different from experimental values, a qualitative look at the overall trend indicates the following for the N3 pK_a series: folate < ADMDF ≪ DMDDF. These calculations suggest that binding of folate and ADMDF may be weaker than for DMDDF as binding of the first two ligands would be accompanied by protonation effects. In contrast, the pK_a for DMDDF is sufficiently high that protonation effects would not be an issue. This hypothesis could also explain why the N^{10}-methyl substitution weakens binding. Poe observed an N3 pK_a of 7.68 for N^{10}-methylfolate [vs 8.38 for folate (*52*)]. The slightly lower pK_a would predict a greater protonation effect involved with binding of N^{10}-methylfolate vs folate. This behavior is observed in our plots of ΔH_{obsd} versus the buffer heat of ionization where the slope for N^{10}-methylfolate is 0.56 while that for folate binding is 0.4. While this analysis only describes a set of five members (including DHF), it suggests that substitutions at NA2 (amine off C2), C2, N5, N8, and N10 are well tolerated by R67 DHFR and that indirect effects that alter the N3 pK_a are more important to binding.

A second observation is that neither aminopterin nor MTX form a ternary complex. As aminopterin does form a binary complex, these altered binding patterns indicate that binary complex binding must differ somewhat from ternary complex binding. Possibilities include alteration of the exact position of the pteridine ring, or different stacking of the pteridine−pteridine vs pteridine−nicotinamide rings, or perhaps flipping of the pteridine ring [as observed when bound MTX is compared to bound folate in chromosomal DHFR (*60*)]. Also, since aminopterin differs from folate by the substitution of an amino group for O4, the inability of aminopterin to form a ternary complex supports a critical role for O4 in productive ternary complex formation.

When the substrate series folate/DHF → pteroic acid/DHP → DHB → pABA-Glu is considered, we find that ternary complex formation is weakened (Tables 3 and 4). The ΔH

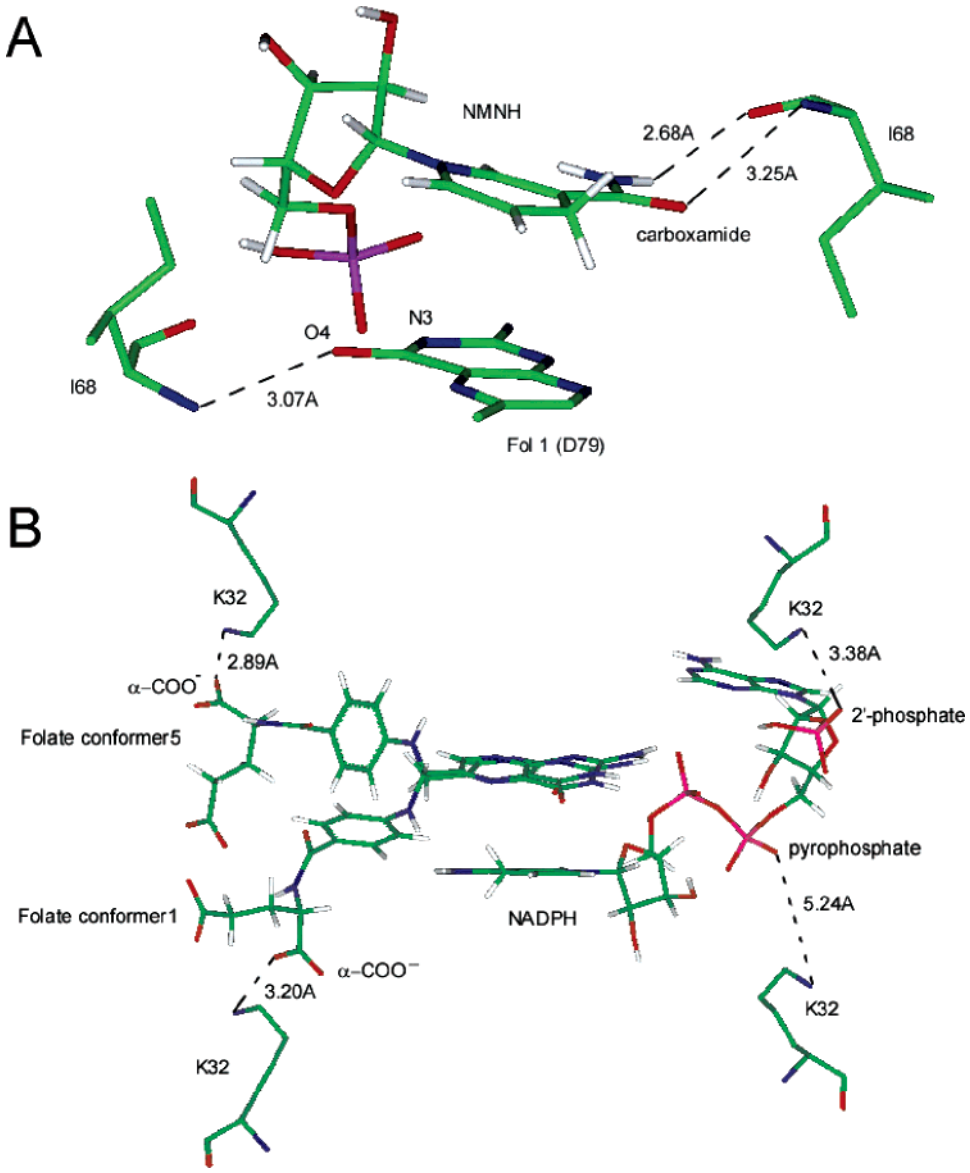

FIGURE 6: A model of the ternary complex. Panel A depicts the position of bound folate (residue D79 in 1VIF) and the top-scoring NMNH conformer obtained from DOCK (*12*). The color code is as follows: carbon atoms, green; nitrogen, blue; oxygen, red; phosphorus, magenta; and hydrogen, white. Selected atoms, potential H-bonds, and their distances are shown. Symmetry-related interactions with the backbone NH and O atoms of I68 appear to serve dual roles in binding, allowing pairing with the O4 atom of folate and the carboxamide group of the cofactor. This image possesses the same orientation as Figure 1 and magnifies the center of the pore. Panel B shows the predicted position of docked NADPH as well as two conformers (1 and 5) of the docked folate (*12*). Here potential ionic interactions with symmetry-related K32 residues are predicted, both for the glutamate tail of folate and for the pyrophosphate and 2′-phosphate groups in NADPH. Stacking of the pteridine and nicotinamide rings occurs in the center of the pore. This image is related to that of Figure 1 by a 90° rotation along the *y*-axis.

effects are more surprising as the enthalpic contribution is clearly provided by the pABA-Glu tail. When it is removed, binding is weakened 33-fold (K_d of DHF vs the K_i of DHB), and the enthalpic contribution of binding cannot be measured by ITC. Further, binding of the pABA-Glu tail does display a small but obvious enthalpic signal, coupled with very weak binding. Since most enthalpic contributions arising from ionic interactions, H-bonds, etc. involve positioning of pairwise interactions or counter charges such that increased rigidity occurs, it is surprising that both crystallography (*4*) and NMR (*8*) studies find that the pABA-Glu tail of bound folate is disordered. These various observations suggest that the ΔH contribution associated with binding folate or DHF comes from a disordered segment of the molecule. As ionic interactions have a $1/r$ distance relationship, perhaps positioning the negatively charged tail between symmetry-related K32 residues on one-half of the pore allows an "average" binding mode that provides a sufficient interaction enthalpy. Alternatively, solvent-separated ion pairs may be occurring to minimize any desolvation penalty (*61*−*63*). This view is also supported by the binding of DHP to R67 DHFR·NADPH, which displays an intermediate enthalpy value, even though the position of the negative charge is different.

Use of alternate cofactors results in weaker binding of folate, indicating interligand pairing preferences. While thio-NADPH addition had minimal effects on binary complex formation, it showed a large effect on ternary complex formation, weakening binding of folate by 7-fold. Also, while AcPADPH does not readily form an enzyme·AcPADPH complex, once bound, it readily allows folate addition. These

observations point to both the amine and carbonyl moieties of the cofactor's carboxamide group being important in formation of the enzyme·cofactor complex as well as stacking with folate.

Which Atoms or Groups Are Important in Binding and Provide Anchoring to the Active Site? To summarize our ITC studies using NADPH analogues and fragments, an important group involved in binding is the nicotinamide moiety, in particular the amine in its carboxamide group. In addition, an effect for the 2′-phosphate on the ribose is observed. From our previous salt effects on binding, there is an additional effect by the pyrophosphate group on binding (*18*, *48*). Finally, a strong preference for a reduced nicotinamide ring was observed both in these results and in previous studies (*6*).

For substrate binding, an important element is the reduction state of the pteridine ring, with a strong preference for the dihydro form. In addition, the preferred binding of the keto form (N3 protonated) of folate points to a strong role for the N3 and/or O4 atoms. The inability of aminopterin to form a ternary complex lends further support to a strong role for O4.

Considering both ITC and K_i results, we find a broad tolerance for substitutions in the Glu side chain of the folyl substrate. Substitution of either a neutral (N^{α}-pteroyl-L-histidine) or a positively charged side chain (N^{α}-pteroyl-L-ornithine) does not greatly alter the K_i value. As the α-carboxylate group remains invariant in these compounds, it likely is the group that interacts with nearby K32 residues. Alternatively, considering only a 3-fold decrease in inhibition by pteroic acid, at least one negative charge is necessary for a pairwise interaction, and some tolerance exists with respect to placement of this charge. A similar pattern has been observed when asymmetric single and double K32M mutations have been engineered into a quadruplicated R67 DHFR gene product; i.e., various topologies of mutations are tolerated and do not have as large effects as would be expected if a single topology of bound DHF occurred (*48*).

Our docked complex model is displayed in Figure 6 to allow comparison with these experimental results. The position of the bound pteridine ring of folate comes from the 1VIF (two folate) structure (*4*), and the predicted positions of NMNH and NADPH were obtained by docking (*12*). Using the docked NMNH structure, the entire folate molecule was redocked to potentially gain additional information concerning the tail position. Two predicted folate conformers are shown. These various docked structures generally agree with the binding results. In particular, direct interactions with protein appear to provide the highest contribution to binding. The two prime examples are the proposed H-bond between O4 of folate and the NH backbone of I68 as well as the predicted H-bonds between the carboxamide of NADPH with the backbone atoms of a symmetry-related I68 residue. Indirect interactions mediated through water (for example, the carbonyl of V66 interacts indirectly with N1 and N8 of folate via a water molecule) appear to correlate with a broader binding tolerance. Panel 6B also depicts the potential interactions between K32 and the phosphate groups of NADPH as well as the α-carboxylate group of folate.

ACKNOWLEDGMENT

We thank an anonymous reviewer for suggesting a potential correlation between the K_d for binding of folate analogues with the N3 pK_a value.

SUPPORTING INFORMATION AVAILABLE

Two figures showing ITC titrations describing binary complex formation with 2-deamino-2-methyl-5,8-dideazafolate as well as ternary complex formation of R67 DHFR−NADPH−pteroyldi-γ-L-glutamate, plus inhibition of R67 DHFR activity by ADMDF. This material is available free of charge via the Internet at http://pubs.acs.org.

REFERENCES

1. Hitchings, G. H., and Burchall, J. J. (1965) Inhibition of folate biosynthesis and function as a basis for chemotherapy, *Adv. Enzymol. Relat. Areas Mol. Biol. 27*, 417−468.
2. Brisson, N., and Hohn, T. (1984) Nucleotide sequence of the dihydrofolate-reductase gene borne by the plasmid R67 and conferring methotrexate resistance, *Gene 28*, 271−274.
3. White, P. A., and Rawlinson, W. D. (2001) Current status of the *aadA* and *dfr* gene cassette families, *J. Antimicrob. Chemother. 47*, 495−496.
4. Narayana, N., Matthews, D. A., Howell, E. E., and Xuong, N. H. (1995) A plasmid-encoded dihydrofolate reductase from trimethoprim-resistant bacteria has a novel D2-symmetric active site, *Nat. Struct. Biol. 2*, 1018−1025.
5. Howell, E. E. (2005) Searching sequence space: Two different approaches to dihydrofolate reductase catalysis, *ChemBioChem 6*, 590−600.
6. Bradrick, T. D., Beechem, J. M., and Howell, E. E. (1996) Unusual binding stoichiometries and cooperativity are observed during binary and ternary complex formation in the single active pore of R67 dihydrofolate reductase, a D2 symmetric protein, *Biochemistry 35*, 11414−11424.
7. Pitcher, W. H., III, DeRose, E. F., Mueller, G. A., Howell, E. E., and London, R. E. (2003) NMR studies of the interaction of a type II dihydrofolate reductase with pyridine nucleotides reveal unexpected phosphatase and reductase activity, *Biochemistry 42*, 11150−11160.
8. Li, D., Levy, L. A., Gabel, S. A., Lebetkin, M. S., DeRose, E. F., Wall, M. J., Howell, E. E., and London, R. E. (2001) Interligand Overhauser effects in type II dihydrofolate reductase, *Biochemistry 40*, 4242−4252.
9. Kuntz, I. D., Blaney, J. M., Oatley, S. J., Langridge, R., and Ferrin, T. E. (1982) A geometric approach to macromolecule-ligand interactions, *J. Mol. Biol. 161*, 269−288.
10. Shoichet, B. K., and Kuntz, I. D. (1993) Matching chemistry and shape in molecular docking, *Protein Eng. 6*, 723−732.
11. Ewing, T. J. A., and Kuntz, I. D. (1997) Critical evaluation of search algorithms for automated molecular docking and database screening, *J. Comput. Chem. 18*, 1175−1189.
12. Howell, E. E., Shukla, U., Hicks, S. N., Smiley, R. D., Kuhn, L. A., and Zavodszky, M. I. (2001) One site fits both: a model for the ternary complex of folate + NADPH in R67 dihydrofolate reductase, a D2 symmetric enzyme, *J. Comput.-Aided Mol. Des. 15*, 1035−1052.
13. Castillo, R., Andres, J., and Moliner, V. (1999) Catalytic mechanism of dihydrofolate reductase enzyme. A combined quantum-mechanical/molecular-mechanical characterization of transition state structure for the hydride transfer step, *J. Am. Chem. Soc. 121*, 12140−12147.
14. Andres, J., Moliner, V., Safont, V. S., Domingo, L. R., Picher, M. T., and Krechl, J. (1996) On transition structures for hydride transfer step: a theoretical study of the reaction catalyzed by dihydrofolate reductase enzyme, *Bioorg. Chem. 24*, 10−18.
15. Park, H., Bradrick, T. D., and Howell, E. E. (1997) A glutamine 67→histidine mutation in homotetrameric R67 dihydrofolate reductase results in four mutations per single active site pore and causes substantial substrate and cofactor inhibition, *Protein Eng. 10*, 1415−1424.

16. Strader, M. B., Chopra, S., Jackson, M., Smiley, R. D., Stinnett, L. G., Wu, J., and Howell, E. E. (2004) Defining the binding site of homotetrameric R67 dihydrofolate reductase and correlating binding enthalpy with catalysis, *Biochemistry 43*, 7403−7412.
17. Strader, M. B., and Howell, E. E. (1997) Stable maintenance of a tandem array of four R67 dihydrofolate reductase genes, *Gibco-BRL Focus 19*, 24−25.
18. Hicks, S. N., Smiley, R. D., Hamilton, J. B., and Howell, E. E. (2003) Role of ionic interactions in ligand binding and catalysis of R67 dihydrofolate reductase, *Biochemistry 42*, 10569−10578.
19. Reece, L. J., Nichols, R., Ogden, R. C., and Howell, E. E. (1991) Construction of a synthetic gene for an R-plasmid-encoded dihydrofolate reductase and studies on the role of the N-terminus in the protein, *Biochemistry 30*, 10895−10904.
20. Gornall, A. G., Bardawill, C. J., and David, M. M. (1949) Determination of serum proteins by means of the biuret reaction, *J. Biol. Chem. 177*, 751−766.
21. Avigad, G. (1979) Reduction of nicotinamide adenine dinucleotides by sodium cyanoborohydride, *Biochim. Biophys. Acta 571*, 171−174.
22. Horecker, B. L., and Kornberg, A. (1948) The extinction coefficients of the reduced band of pyridine nucleotides, *J. Biol. Chem. 175*, 385−390.
23. Tischler, M. E., and Fisher, R. R. (1973) Oxidation of reduced nicotinamide hypoxanthine dinucleotide phosphate by intact rat liver mitochondria, *Biochim. Biophys. Acta 305*, 199−205.
24. Trimboli, A. J., and Barber, M. J. (1994) Assimilatory nitrate reductase: reduction and inhibition by NADH/NAD^+ analogs, *Arch. Biochem. Biophys. 315*, 48−53.
25. Smith, S. L., and Burchall, J. J. (1983) Alpha-pyridine nucleotides as substrates for a plasmid-specified dihydrofolate reductase, *Proc. Natl. Acad. Sci. U.S.A. 80*, 4619−4623.
26. Morrison, J., and Stone, S. (1988) Mechanism of the reaction catalyzed by DHFR from *E. coli*: pH and deuterium isotope effects with NADPH as the variable substrate, *Biochemistry 27*, 5499−5506.
27. Blakley, R. L. (1960) Crystalline dihydropteroylglutamic acid, *Nature 188*, 231−232.
28. Prabhu, V., Lui, H., and King, J. (1997) Arabidopsis dihydropteroate synthase: general properties and inhibition by reaction product and sulfonamides, *Phytochemistry 45*, 23−27.
29. Rosowsky, A., Bader, H., and Forsch, R. A. (1989) Synthesis of the folylpolyglutamate synthetase inhibitor N-pteroyl-L-ornithine and its N-benzoyl and N-hemiphthaloyl derivatives, and an improved synthesis of N-(4-amino-4-deoxypteroyl)-N-hemiphthaloyl-L-ornithine, *Pteridines 1*, 91−98.
30. Rosowsky, A., Forsch, R., and Moran, R. G. (1992) N-[4-[[3,4-Dihydro-4-oxo-1,2,3-benzotriazin-6-yl)methyl]amino]benzoyl]-L-glutamic acid, a novel A-ring analogue of 2-desamino-5,8-dideazafolic acid, *J. Med. Chem. 35*, 2626−2630.
31. Rosowsky, A., Forsch, R. A., and Moran, R. G. (1989) (6R,6S)-5,8,10-trideaza-5,6,7,8-tetrahydrofolate and (6R,6S)-5,8,10-trideaza-5,6,7,8-tetrahydropteroyl-L-ornithine as potential antifolates and antitumor agents, *J. Med. Chem. 32*, 709−715.
32. Rosowsky, A., Forsch, R. A., Null, A., and Moran, R. G. (1999) 5-deazafolate analogues with a rotationally restricted glutamate or ornithine side chain: synthesis and binding interaction with folylpolyglutamate synthetase, *J. Med. Chem. 42*, 3510−3519.
33. Rosowsky, A., Forsch, R. A., Reich, V. E., Freisheim, J. H., and Moran, R. G. (1992) Side chain modified 5-deazafolate and 5-deazatetrahydrofolate analogues as mammalian folylpolyglutamate synthetase and glycinamide ribonucleotide formyltransferase inhibitors: synthesis and in vitro biological evaluation, *J. Med. Chem. 35*, 1578−1588.
34. Mao, Z., Pan, J., and Kalman, T. I. (1996) Design and synthesis of histidine analogues of folic acid and methotrexate as potential folylpolyglutamate synthetase inhibitors, *J. Med. Chem. 39*, 4340−4344.
35. Blakley, R. L. (1969) in *Frontiers of Biology: The Biochemistry of Folic Acid and Related Pteridines* (Neuberger, A., and Tatum, F. L., Eds.) pp 58−105, North-Holland Publishing Co., Amsterdam.
36. Temple, C., Jr., and Montgomery, J. A. (1984) in *Folates and Pterins: Chemistry and Biochemistry of Folates* (Blakley, R. L., and Benkovic, S. J., Eds.) pp 61−120, John Wiley and Sons, New York.
37. Williams, E. A., and Morrison, J. F. (1992) Human dihydrofolate reductase: reduction of alternative substrates, pH effects, and inhibition by deazafolates, *Biochemistry 31*, 6801−6811.
38. Godwin, H. A., Rosenberg, I. H., Ferenz, C. R., Jacobs, P. M., and Meienhofer, J. (1972) The synthesis of biologically active pteroyloligo-gamma-L-glutamates (folic acid conjugates). Evaluation of (3H)-pteroylheptaglutamate for metabolic studies, *J. Biol. Chem. 247*, 2266−2271.
39. Pfleiderer, W. (1985) in *Folates and Pterins: Chemistry and Biochemistry of Pterins* (Blakley, R. L., and Benkovic, S. J., Eds.) pp 43−114, John Wiley and Sons, New York.
40. Shiota, T., Disraely, M. N., and McCann, M. P. (1964) The enzymatic synthesis of folate-like compounds from hydroxymethyldihydropteridine pyrophosphate, *J. Biol. Chem. 239*, 2259−2266.
41. Poe, M. (1973) Proton magnetic resonance studies of folate, dihydrofolate, and methotrexate. Evidence from pH and concentration studies for dimerization, *J. Biol. Chem. 248*, 7025−7032.
42. Wiseman, T., Williston, S., Brandts, J. F., and Lin, L. N. (1989) Rapid measurement of binding constants and heats of binding using a new titration calorimeter, *Anal. Biochem. 179*, 131−137.
43. Fukada, H., and Takahashi, K. (1998) Enthalpy and heat capacity changes for the proton dissociation of various buffer components in 0.1 M potassium chloride, *Proteins 33*, 159−166.
44. Ellis, K. J., and Morrison, J. F. (1982) Buffers of constant ionic strength for studying pH-dependent processes, *Methods Enzymol. 87*, 405−426.
45. Jelesarov, I., and Bosshard, H. R. (1994) Thermodynamics of ferredoxin binding to ferredoxin:$NADP^+$ reductase and the role of water at the complex interface, *Biochemistry 33*, 13321−13328.
46. Segel, I. H. (1975) *Enzyme Kinetics: Behavior and Analysis of Rapid Equilibrium and Steady State Enzyme Systems*, John Wiley and Sons, New York.
47. Smiley, R. D., Saxton, A. M., Jackson, M. J., Hicks, S. N., Stinnett, L. G., and Howell, E. E. (2004) Nonlinear fitting of bisubstrate enzyme kinetic models using SAS computer software: application to R67 dihydrofolate reductase, *Anal. Biochem. 334*, 204−206.
48. Hicks, S. N., Smiley, R. D., Stinnett, L. G., Minor, K. H., and Howell, E. E. (2004) Role of Lys-32 residues in R67 dihydrofolate reductase probed by asymmetric mutations, *J. Biol. Chem. 279*, 46995−47002.
49. Lafitte, D., Lamour, V., Tsvetkov, P. O., Makarov, A. A., Klich, M., Deprez, P., Moras, D., Briand, C., and Gilli, R. (2002) DNA gyrase interaction with coumarin-based inhibitors: the role of the hydroxybenzoate isopentenyl moiety and the 5′-methyl group of the noviose, *Biochemistry 41*, 7217−7223.
50. Freel Meyers, C. L., Oberthur, M., Xu, H., Heide, L., Kahne, D., and Walsh, C. T. (2004) Characterization of NovP and NovN: completion of novobiocin biosynthesis by sequential tailoring of the noviosyl ring, *Angew. Chem., Int. Ed. Engl. 43*, 67−70.
51. Ortiz-Salmeron, E., Yassin, Z., Clemente-Jimenez, M. J., Las Heras-Vazquez, F. J., Rodriguez-Vico, F., Baron, C., and Garcia-Fuentes, L. (2001) Thermodynamic analysis of the binding of glutathione to glutathione S-transferase over a range of temperatures, *Eur. J. Biochem. 268*, 4307−4314.
52. Poe, M. (1977) Acidic dissociation constants of folic acid, dihydrofolic acid, and methotrexate, *J. Biol. Chem. 252*, 3724−3728.
53. Kallen, R. G., and Jencks, W. P. (1966) The dissociation constants of tetrahydrofolic acid, *J. Biol. Chem. 241*, 5845−5850.
54. Maharaj, G., Selinsky, B. S., Appleman, J. R., Perlman, M., London, R. E., and Blakley, R. L. (1990) Dissociation constants for dihydrofolic acid and dihydrobiopterin and implications for mechanistic models for dihydrofolate reductase, *Biochemistry 29*, 4554−4560.
55. Deng, H., Callender, R., and Howell, E. (2001) Vibrational structure of dihydrofolate bound to R67 dihydrofolate reductase, *J. Biol. Chem. 276*, 48956−48960.
56. Miller, B. G., Snider, M. J., Short, S. A., and Wolfenden, R. (2000) Contribution of enzyme-phosphoribosyl contacts to catalysis by orotidine 5′-phosphate decarboxylase, *Biochemistry 39*, 8113−8118.
57. Stout, T. J., Sage, C. R., and Stroud, R. M. (1998) The additivity of substrate fragments in enzyme-ligand binding, *Structure 6*, 839−848.
58. Leigh, D. A. (2003) Summing up ligand binding interactions, *Chem. Biol. 10*, 1143−1144.
59. Perrin, D., Dempsey, B., and Serjeant, E. (1981) pK_a Prediction for Organic Acids and Bases, Chapman and Hall, London.

60. Bolin, J., Filman, D., Matthews, D., Hamlin, R., and Kraut, J. (1982) Crystal structures of *Escherichia* coli and *Lactobacillus casei* dihydrofolate reductase refined at 1.7 Å resolution. I. General features and binding of methotrexate, *J. Biol. Chem. 257*, 13650−13662.
61. Chong, L. T., Dempster, S. E., Hendsch, L. P., and Tidor, B. (1998) Computation of electrostatic complements to proteins: a case of charge stabilized binding, *Protein Sci. 7*, 206−210.
62. Dougherty, R. C., and Howard, L. N. (2003) Alkaline-earth metals in a box: structures of solvent-separated ion pairs, *Biophys. Chem. 105*, 269−278.
63. Joughin, B. A., Green, D. F., and Tidor, B. (2005) Action-at-a-distance interactions enhance protein binding affinity, *Protein Sci. 14*, 131−139.

BI050881S